

# DMRadio-m<sup>3</sup>: A Search for the QCD Axion Below 1 $\mu\text{eV}$

L. Brouwer,<sup>1</sup> S. Chaudhuri,<sup>2</sup> H.-M. Cho,<sup>3</sup> J. Corbin,<sup>4</sup> W. Craddock,<sup>3</sup> C. S. Dawson,<sup>4</sup> A. Droster,<sup>5</sup>  
J. W. Foster,<sup>6</sup> J. T. Fry,<sup>7</sup> P. W. Graham,<sup>4</sup> R. Henning,<sup>8,9</sup> K. D. Irwin,<sup>4,3,\*</sup> F. Kadribasic,<sup>4</sup>  
Y. Kahn,<sup>10</sup> A. Keller,<sup>5</sup> R. Kolevator,<sup>2</sup> S. Kuenstner,<sup>4</sup> A. F. Leder,<sup>5,1</sup> D. Li,<sup>3</sup> J. L. Ouellet,<sup>7,†</sup>  
K. M. W. Pappas,<sup>7</sup> A. Phipps,<sup>11</sup> N. M. Rapidis,<sup>4</sup> B. R. Safdi,<sup>12</sup> C. P. Salemi,<sup>7</sup> M. Simanovskaia,<sup>4</sup> J. Singh,<sup>4</sup>  
E. C. van Assendelft,<sup>4</sup> K. van Bibber,<sup>5</sup> K. Wells,<sup>4</sup> L. Winslow,<sup>7</sup> W. J. Wisniewski,<sup>3</sup> and B. A. Young<sup>13</sup>  
(DMRadio Collaboration)

<sup>1</sup>*Accelerator Technology and Applied Physics Division,*

*Lawrence Berkeley National Laboratory, Berkeley, CA 94720*

<sup>2</sup>*Department of Physics, Princeton University, Princeton, NJ 08544*

<sup>3</sup>*SLAC National Accelerator Laboratory, Menlo Park, CA 94025*

<sup>4</sup>*Department of Physics, Stanford University, Stanford, CA 94305*

<sup>5</sup>*Department of Nuclear Engineering, University of California, Berkeley, Berkeley, CA 94720*

<sup>6</sup>*Center for Theoretical Physics, Massachusetts Institute of Technology, Cambridge, MA 02139*

<sup>7</sup>*Laboratory of Nuclear Science, Massachusetts Institute of Technology, Cambridge, MA 02139*

<sup>8</sup>*Department of Physics and Astronomy, University of North Carolina,  
Chapel Hill, Chapel Hill, North Carolina, 27599*

<sup>9</sup>*Triangle Universities Nuclear Laboratory, Durham, NC 27710*

<sup>10</sup>*Department of Physics, University of Illinois at Urbana-Champaign, Urbana, IL 61801*

<sup>11</sup>*Department of Physics, California State University, East Bay, Hayward, CA 94542*

<sup>12</sup>*Department of Physics, University of California, Berkeley, Berkeley, CA 94720*

<sup>13</sup>*Department of Physics, Santa Clara University, Santa Clara, CA 95053*

(Dated: April 28, 2022)

The QCD axion is one of the most compelling candidates to explain the dark matter abundance of the universe. With its extremely small mass ( $\ll 1 \text{ eV}/c^2$ ), axion dark matter interacts as a classical field rather than a particle. Its coupling to photons leads to a modification of Maxwell's equations that can be measured with extremely sensitive readout circuits. DMRadio-m<sup>3</sup> is a next-generation search for axion dark matter below 1  $\mu\text{eV}$  using a 4 T static magnetic field, a coaxial inductive pickup, a tunable LC resonator, and a DC-SQUID readout. It is designed to search for QCD axion dark matter over the range  $20 \text{ neV} \lesssim m_a c^2 \lesssim 800 \text{ neV}$  ( $5 \text{ MHz} < \nu < 200 \text{ MHz}$ ) with at least KSVZ sensitivity over the full range, and DFSZ sensitivity above  $m_a c^2 \approx 120 \text{ neV}$  (30 MHz) with a 5 year scan time. In this letter, we present a baseline design and sensitivity for DMRadio-m<sup>3</sup>.

## I. INTRODUCTION

The Strong CP problem describes an unnaturally fine-tuned symmetry of nature that suggests an explanation beyond the Standard Model (SM) of particle physics. The leading solution to this problem is the introduction of a new Peccei-Quinn symmetry, which is spontaneously broken at some high energy scale  $f_a$ , and produces a new pseudo-Goldstone boson, the axion  $a$  [1–4]. Interactions with quantum chromodynamics (QCD) give the axion field a non-trivial potential, which has the effect of i) solving the Strong CP problem, ii) giving the axion a mass,  $m_a c^2 \approx 5.7 \text{ neV} (10^{15} \text{ GeV}/f_a)$  [5], and iii) producing a relic abundance of axions in the early universe that satisfy all the conditions to be dark matter (DM) [6–8]. Over the last few years, the axion has emerged as one of the leading DM candidates.

Recent theoretical work has opened up a wide range of interesting parameter space for both QCD axion and

axion-like particle (ALP) models [9–13]. In particular, the mass range  $1 \text{ neV} \lesssim m_a c^2 \lesssim 1 \mu\text{eV}$  is interesting for grand unification theories (GUTs) [11, 14–22], String Theory models [23–30], and naturalness arguments [12, 31]. Other ALP models make predictions in this mass range for simultaneously explaining both the DM abundance as well as the matter-antimatter asymmetry [32].

Due to its small mass and cold production in the early universe, axion dark matter (ADM) has a very high per-state occupation number and interacts as a classical field making it wave-like DM. Depending on the precise model, the axion may couple to any of the SM particles, but one of the least model-dependent couplings is the axion-photon coupling  $g_{a\gamma\gamma}$  [14]. For the QCD axion,  $g_{a\gamma\gamma}$  is directly proportional to  $m_a$ . The uncertainty in the proportionality constant is represented by the Kim–Shifman–Vainshtein–Zakharov (KSVZ) [33, 34] and Dine–Fischler–Srednicki–Zhitnitsky (DFSZ) [35, 36] models, which span about an order of magnitude in uncertainty in  $g_{a\gamma\gamma}$ . A more generic class of ALPs break this proportionality and can have a wide parameter space of possible masses and  $g_{a\gamma\gamma}$  coupling.

The axion-photon coupling produces a modified

\* [irwin@stanford.edu](mailto:irwin@stanford.edu)

† [ouelletj@mit.edu](mailto:ouelletj@mit.edu)

Ampère's law in vacuum

$$\nabla \times \mathbf{B} = \frac{1}{c^2} \frac{\partial \mathbf{E}}{\partial t} - g_{a\gamma\gamma} \sqrt{\frac{\hbar \epsilon_0}{c}} \left( \mathbf{E} \times \nabla a - \frac{\partial a}{\partial t} \mathbf{B} \right), \quad (1)$$

with  $\mathbf{E}$ ,  $\mathbf{B}$  and  $a(x, t)$  representing the electric, magnetic, and axion fields [37]. In the Standard Halo Model (SHM) [38], the axion field is expected to be smooth and, to a good approximation, the  $\nabla a$  term can be neglected. The axion modifications can therefore be treated as an effective volume current  $\mathbf{J}_{\text{eff}} = g_{a\gamma\gamma} \frac{\sqrt{\hbar c}}{\mu_0} \partial_t a \mathbf{B}$ . Assuming the axion accounts for the full DM density, the effective current can be written as

$$\mathbf{J}_{\text{eff}} \approx g_{a\gamma\gamma} \frac{\sqrt{\hbar c}}{\mu_0} \sqrt{2\rho_{\text{DM}}} \cos\left(\frac{m_a c^2 t}{\hbar}\right) \mathbf{B}, \quad (2)$$

with local DM density  $\rho_{\text{DM}} \approx 0.45 \text{ GeV}/\text{cm}^3$  [39] and an axion frequency  $\nu_a = m_a c^2 / (2\pi\hbar)$ . A powerful approach to searching for ADM is to deploy a large, static  $\mathbf{B}$ -field to drive  $\mathbf{J}_{\text{eff}}$  through a pickup structure and search for excess power in a narrow bandwidth  $\Delta\nu_{\text{sig}}/\nu_a \approx 10^{-6}$  [38].

Historically, ADM experiments have focused on probing the mass range  $1 \mu\text{eV} \lesssim m_a c^2 \lesssim 40 \mu\text{eV}$  with microwave cavities [40–47], where the Compton wavelength of the axion is able to resonantly excite a cavity mode. However, the cavity resonance condition requires a characteristic detector size  $L$  comparable to the axion Compton wavelength,  $m_a L / (\hbar c) \sim 1$ , and makes probing masses below  $1 \mu\text{eV}$  (wavelengths larger than  $\sim 1 \text{ m}$ ) impractical. However, at lower axion masses, the magneto-quasistatic (MQS) limit applies and  $\mathbf{J}_{\text{eff}}$  can be treated as generating secondary magnetic fields, which can be detected with an inductive pickup and enhanced with a lumped element resonator [48–52]. This has been experimentally realized with a toroidal magnet geometry with the ABRACADABRA-10 cm prototype [53–55] and SHAFT [56] and in a solenoidal geometry with ADMX-SLIC [57] and the BASE Penning trap [58]. DMRadio-Pathfinder has also performed a resonant search for dark photons (DPs) in the MQS regime with the solenoidal pickup geometry [59]. In this letter, we present an optimized lumped-element experimental design called DMRadio-m<sup>3</sup>, capable of probing ADM over the mass range  $20 \text{ neV} \lesssim m_a c^2 \lesssim 800 \text{ neV}$  ( $5 \text{ MHz} < \nu < 200 \text{ MHz}$ ) with a 5 yr scan time, achieving DFSZ sensitivity for masses above  $\sim 120 \text{ neV}/c^2$  (30 MHz).

## II. LUMPED ELEMENT DETECTION

The technical challenge facing any ADM experiment is one of signal-to-noise power. As highlighted in [60], the ADM field contains enough power per square meter to illuminate an LED, but non-optimal impedance matching implies that any practical receiver will only be able to extract a tiny fraction of this power. Resonant circuits – either microwave cavities or LC lumped element circuits

– have much lower impedance on resonance and are thus able to extract more power from the axion field.

For an arbitrary inductive pickup coupled to an  $\mathbf{J}_{\text{eff}}$ , the voltage across the inductor can be expressed as

$$|\tilde{V}_{pp}|^2 = 4g_{a\gamma\gamma}^2 \rho_{\text{DM}} \left( \frac{c^5}{\hbar \mu_0} \right) m_a^2 c_{\text{PU}}^2 L_{\text{PU}} B_0^2 V_{\text{PU}}^{5/3} \quad (3)$$

(see Appendix A). Here  $B_0$  and  $V_{\text{PU}}$  are the characteristic magnetic field and volume of the pickup,  $L_{\text{PU}}$  is its inductance, and  $c_{\text{PU}}$  is a dimensionless proportionality constant that depends on the detector geometry and flux coupling.

When coupled to a capacitor, the impedance of the resulting circuit  $Z_L(\nu)$  is significantly decreased at the resonance frequency,  $\nu_r$ . If  $\nu_r$  is tuned close to the axion driving frequency  $\nu_r \approx m_a c^2 / (2\pi\hbar)$ , the current driven through the circuit from axion conversion,  $\tilde{I}_{\text{sig}}$ , can be enhanced by multiple orders of magnitude – typically expressed in terms of the resonator quality factor  $Q$ :

$$\begin{aligned} |\tilde{I}_{\text{sig}}|^2 &= \frac{|\tilde{V}_{pp}|^2}{|Z(\nu)|^2} \\ &= 4g_{a\gamma\gamma}^2 \rho_{\text{DM}} \left( \frac{c^5}{\hbar \mu_0} \right) \frac{c_{\text{PU}}^2 B_0^2 V_{\text{PU}}^{5/3}}{L_{\text{PU}}} \left( \frac{Q^2}{1 + (2Q\Delta)^2} \right) \end{aligned} \quad (4)$$

which holds for resonator tunings close to the axion driving frequency ( $\Delta \ll 1$ ), and assumes that the pickup dominates the inductance of the circuit. The signal is shaped by the Lorentzian response of the resonator circuit and depends on the fractional detuning of the resonance frequency from the axion frequency,  $\Delta = (2\pi\hbar\nu_r - m_a c^2) / m_a c^2$ . This behavior gives the resonator its characteristic line width,  $\Delta\nu_r = \nu_r / Q$ .

The experimental sensitivity for a resonant search is determined by its scan rate: the rate at which one can scan through frequencies searching for this signal current,  $\tilde{I}_{\text{sig}}$ , in Eqn. 4. The scan rate will be set by the  $g_{a\gamma\gamma}$  sensitivity and the signal-to-noise ratio (SNR) the experiment intends to reach at any particular resonator tuning, as well as the current noise  $|\tilde{I}_N|^2$  at that frequency. At a single resonator tuning, the integration time,  $\tau$ , required to achieve this SNR at  $g_{a\gamma\gamma}$  is given by a modified form of the Dicke radiometer equation

$$\text{SNR}(\nu) = \frac{|\tilde{I}_{\text{sig}}|^2}{|\tilde{I}_N(\nu)|^2} \sqrt{\tau \Delta\nu_{\text{sig}}}. \quad (5)$$

Here  $\Delta\nu_{\text{sig}}$  is the spectral width of the axion signal, which we will assume to follow the SHM throughout the rest of this text,  $\Delta\nu_{\text{sig}}/\nu_a \sim 10^6$ . The current noise  $|\tilde{I}_N(\nu)|^2$  is dominated by thermal Johnson-Nyquist noise and the noise of the first stage amplifier,  $\eta_A(\nu)$ . The amplifier noise consists of both the imprecision and backaction noise (see Appendix A).

For an experimental search with many discrete resonator tunings, this scan rate can be approximated by

the continuous function

$$\frac{d \log \nu_r}{dt} = \pi(6.4 \times 10^5) \left( \frac{c^2}{\mu_0^2} \right) \frac{g_{a\gamma\gamma}^4 \rho_{\text{DM}}^2}{\text{SNR}^2 \nu_r} \times \quad (6)$$

$$c_{\text{PU}}^4 Q B_0^4 V_{\text{PU}}^{10/3} \bar{\mathcal{G}}(\nu_r, k_B T, \eta_A(\nu_r))$$

The  $\bar{\mathcal{G}}(\nu_r, k_B T, \eta_A(\nu_r))$  term is a dimensionless factor that defines the effect of the amplifier matching circuit on the scan rate (see Appendix A). Explicitly, it is a trade-off between the signal gain, described by the Lorentzian, and the frequency dependent system noise. Together, these two set the sensitivity bandwidth,  $\Delta\nu_{\text{sens}}$ , which determines the distance in frequency domain between adjacent resonator tunings. Since the thermal noise and amplifier backaction components follow the same Lorentzian line-shape as the signal gain (i.e. since thermal noise temperature  $k_B T$  is independent of frequency), if it were the only noise source, we would have constant SNR over all frequencies and our tuning step size  $\Delta\nu_{\text{sens}}$  could grow arbitrarily large. However, at frequencies sufficiently far from  $\nu_r$ , the imprecision noise from the first stage amplifier begins to dominate, decreasing the SNR. For a scattering-mode matching circuit tuned for optimal power transfer at a single frequency, the sensitivity bandwidth nearly matches the resonator line width,  $\Delta\nu_{\text{sens}} \approx \nu_r/Q$ . Alternatively, for a matching circuit tuned for optimal scan speed, the scan rate can be significantly improved by modestly reducing on-resonance SNR for a larger  $\Delta\nu_{\text{sens}}$ .

For an optimally matched circuit in the thermal noise limit,  $\bar{\mathcal{G}}$  approximately evaluates to  $\bar{\mathcal{G}}(\nu_r, k_B T, \eta) \approx 2\pi\hbar\nu_r(6\sqrt{3}k_B T\eta)^{-1}$ .

### III. DETECTOR DESIGN

DMRadio-m<sup>3</sup> uses a static 4 T solenoid magnet to drive  $\mathbf{J}_{\text{eff}}$  along the axis of a coaxial inductive pickup (see Fig. 1b.) The coaxial pickup couples to a tunable capacitor to form an LC resonator circuit, targeting a resonator quality factor of  $Q > 10^5$ . The circuit is readout by conventional DC-SQUIDS with a noise level 20 times the standard quantum limit (SQL). The coaxial pickup and capacitor are cooled to an operating temperature of  $T \approx 20$  mK, while the magnet is maintained at 4 K. We discuss each of these terms in detail below.

DMRadio-m<sup>3</sup> builds on the experience of ABRACADABRA-10 cm, DMRadio-Pathfinder, and DMRadio-50L (currently under construction.) All three detectors use a superconducting inductive pickup to search for ADM or DPs below 20 neV. DMRadio-Pathfinder and DMRadio-50L [61] both utilize a resonant readout approach, and ABRACADABRA-10 cm and DMRadio-50L both utilize a toroidal magnet geometry. The toroidal magnet geometry works particularly well at low frequencies (i.e. low axion masses) because it completely contains the magnetic field, allowing the use of lossless superconducting materials. Loss is only introduced through coupling

to lossy external materials near the detector, which can be efficiently screened. However, at frequencies above  $\sim 50$  MHz, irreducible stray capacitances associated with reading out the axion current begins to short the signal and rapidly reduce the signal sensitivity at higher frequencies [62]. Hence, a change of geometry is required to probe higher axion masses.

DMRadio-m<sup>3</sup> uses a solenoid magnet, with a bore volume of  $V \approx 2 \text{ m}^3$ , and a characteristic field of  $B_0 = 4 \text{ T}$ . This geometry creates a large-volume, high-field region and drives  $\mathbf{J}_{\text{eff}}$  along the axis of the solenoid (see Fig. 1a.) Unlike the toroid, the solenoid topology exposes the magnetic field, requiring that the inductive pickup sit in the large primary field. Because SQUID amplifiers cannot operate in such a field, DMRadio-m<sup>3</sup> uses a set of bucking coils to bend the field lines outward, producing a low-field region directly above the high-field region. The resulting magnetic field has significant variation within the bore of the magnet, reaching a peak value of  $\approx 7 \text{ T}$  far off-axis; but with a characteristic value of  $B_0 = 4 \text{ T}$  along the central axis in the high-field region. The low-field region sits only 20 cm above the high-field region and has a peak field value of  $|\mathbf{B}| \lesssim 400 \text{ mT}$  (see Fig. 1c). These remaining fields will be further reduced with additional bucking coils and superconducting shielding.

TABLE I. DMRadio-m<sup>3</sup> detector parameter targets.

Parameter	Target Value	
Geometric Factor	$c_{\text{PU}}$	0.18
Magnetic Field	$B_0$	$> 4 \text{ T}$
Pickup Volume	$V_{\text{PU}}$	$1.25 \text{ m}^3$
Quality Factor	$Q$	$> 10^5$
Pickup Temperature	$T$	$< 20 \text{ mK}$
Amplifier Noise	$\eta_A$	$< 20$

DMRadio-m<sup>3</sup> detects the axion-induced  $\mathbf{J}_{\text{eff}}$  via a coaxial inductive pickup, placed in the high-field region of the magnet (see Fig. 1a). The coaxial geometry maximizes the coupling to  $\mathbf{J}_{\text{eff}}$ , while minimizing the pickup inductance  $L_{\text{PU}}$ . Because it sits inside of the magnetic field, it is challenging to make the inductive pickup superconducting and therefore lossless. Instead, the pickup is made from oxygen-free, high-conductivity (OFHC) copper. The finite conductivity of copper sets an upper limit on the achievable quality factor of the LC resonator. At the frequencies relevant for DMRadio-m<sup>3</sup> and at temperatures  $< 100 \text{ mK}$ , the anomalous surface resistance of copper is lower than at  $\sim \text{GHz}$  frequencies and, combined with the large volume-to-surface ratio, the resonator goal of  $Q > 10^5$  is achievable.

While the inductive pickup can sit in the primary field without unacceptably degrading  $Q$ , the same does not extend to the tunable capacitor, which must be superconducting, or to the SQUIDS, which require an ultra-low field to operate. Instead, these are placed in the low-field region above the coaxial pickup. To bridge the distance between the pickup and the low-field region without in-

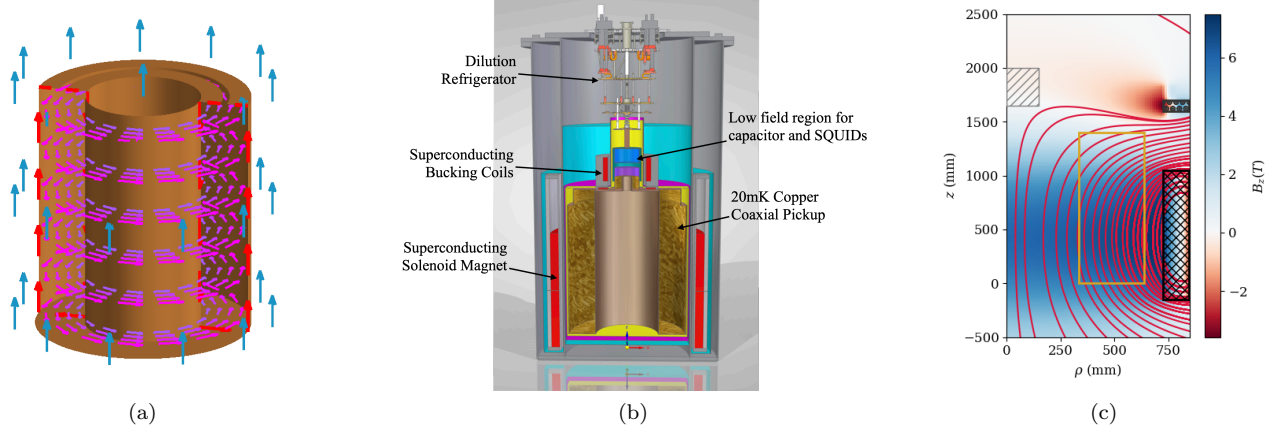


FIG. 1. Left: Simplified cartoon of the DMRadio- $m^3$  coaxial pickup to demonstrate current and magnetic field lines. The solenoid magnet (not shown) drives an oscillating  $J_{\text{eff}}$  (blue arrows) along the axis of the coax. This drives an azimuthal magnetic field (purple arrows), which drives a response current along the walls of the coax (red arrows). The response current is read out across the slit on the top of the coax. Middle: Cross section diagram of DMRadio- $m^3$  with important components labeled. Total height is  $\sim 2.5$  m. Right: Conceptual design for magnetic field profile that balances the need for a high field across the volume of the coaxial inductive pickup region (gold box), while keeping the sensitive electronics free of the field (gray dashed region). Color shading represents the vertical component on the primary field  $B_z$ , while the red lines indicate the magnetic field flux lines. The field is generated by the primary solenoid coils in the black hashed region, and bucking coils with counter flowing current in the black dotted region.

Introducing excessive parasitic inductance, the coax funnels up to a narrow neck that is coupled to the matching circuit above. In order to probe the mass range from  $20 \text{ neV} \lesssim m_a c^2 \lesssim 800 \text{ neV}$ , DMRadio- $m^3$  uses a set of interchangeable coaxial pickups that are exchanged during the run of the experiment. The coaxial pickups are currently being designed, and aim to keep  $C_{\text{PU}}$  &  $V_{\text{PU}}$  maximized over the entire search range, while avoiding resonant modes that may short our signal.

The matching circuit must optimally couple to the pickup and convey the signal to the SQUID readout (see Fig. 2) and consists of the coupling transformer, a tunable capacitor and the inductive coupling to the SQUID amplifier. The signal flux  $\Phi$  couples to the pickup inductance  $L_{\text{PU}}$ , and any additional inductance in the circuit reduces the coupled power. In the series transformer configuration of [49, 50], the coupled axion power is maximized by making the transformer inductance  $L_0 \ll L_{\text{PU}}$ , which is technically challenging given the target  $L_{\text{PU}}$  values of  $\lesssim 200 \text{ nH}$ . However, in the parallel transformer configuration of Fig. 2, we maximize the axion signal power by making the transformer inductance  $L_0 \gg L_{\text{PU}}$ , which is much more realistic and can be achieved with a transformer inductance of  $L_0 \gtrsim 1 \mu\text{H}$ .

The baseline tunable capacitor consists of an array of parallel superconducting plates and sapphire dielectrics. The tuning must be able to scan the range  $10 \text{ pF} \lesssim C \lesssim 5 \text{ nF}$  with part-per-million (ppm) stepping precision. This can be achieved by using a multiple capacitor design with a coarse tuning to give a large enough capacitance swing to cover the full frequency range, and a fine tuning to give ppm frequency precision. If the loss in the

sapphire dielectric proves to be too large, degrading the resonator  $Q$  to an unacceptable level, a fallback option includes removing the dielectric plates and using movable superconducting capacitor plates alone. The design of the tunable capacitor will build off the one currently under construction for DMRadio-50L where many of these questions are being addressed.

Finally, the signal is amplified and read out through a phase-insensitive DC SQUID readout. To maximize the frequency-integrated sensitivity to the axion signal, the coupling transformer coefficient  $\kappa$  must achieve an optimal tradeoff between imprecision and backaction noise. This optimization is worked out for a simple series circuit in detail in [63]. For the sensitivity projections presented here, we target an amplifier noise level of  $\eta_A = 20$ , i.e.  $20\times$  the SQL, which has been demonstrated in [64] (see Appendix A).

The optimal coupling  $\kappa$  is in general frequency dependent, reflecting the fact that at  $T \approx 20 \text{ mK}$  we have a significant frequency dependence on the number of thermal noise photons,  $n_T = (\exp(2\pi\hbar\nu/k_B T) - 1)^{-1}$ , which vary from  $n_T \approx 90$  at  $5 \text{ MHz}$  to  $n_T \approx 2$  at  $200 \text{ MHz}$ . Therefore, DMRadio- $m^3$  is currently designing a transformer capable of *in situ* variation of the coupling strength to maintain optimal matching to the readout amplifier.

The entire pickup structure is cooled to  $T \approx 20 \text{ mK}$  using a dilution refrigerator (DR), while the magnet is held at  $4 \text{ K}$ . With an experimental volume of  $> 1 \text{ m}^3$  and sufficient cooling power to cool the largest coax pickup, the DMRadio- $m^3$  DR will be among the largest in the world. Though, DRs of this size and with lower tempera-



tures have been built previously for  $0\nu\beta\beta$  decay searches [65, 66]. The current plan will locate DMRadio- $m^3$  in Building 750 at SLAC National Accelerator Laboratory, the former site of the SLD detector.

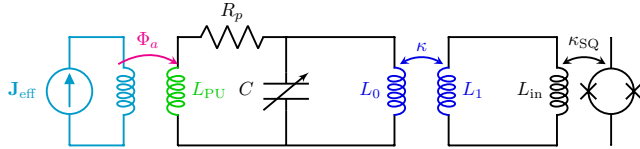


FIG. 2. Effective circuit model for DMRadio- $m^3$ . The axion effective current  $\mathbf{J}_{\text{eff}}$ , is inductively coupled to a coaxial pickup,  $L_{\text{PU}}$ , which, along with a tunable capacitor,  $C$ , form the resonant circuit. A tunable inductive transformer  $\kappa$  couples the signal to the SQUID amplifier. Loss in the readout is represented by resistor,  $R_p$ . On resonance,  $\nu_r^2 \approx (2\pi L_{\text{PU}} C)^{-1}$ , the circuit impedance drops and power is efficiently transferred from the axion field to the receiver.

#### IV. SENSITIVITY

DMRadio- $m^3$  will scan the full range  $20 \text{ neV} \lesssim m_a c^2 \lesssim 800 \text{ neV}$  ( $5 \text{ MHz} < \nu < 200 \text{ MHz}$ ) in stages, by sequentially stepping through a series of  $\sim 5$  detector configurations, each with a different coaxial pickup.

The projected sensitivity for DMRadio- $m^3$  is shown in Fig. 3 compared to the sensitivity of the upcoming DMRadio-50L, which will be described in future publications. The shape of the sensitivity reach is set by the chosen scan strategy, which aims to cover the full frequency range from  $5 \text{ MHz} < \nu_r < 200 \text{ MHz}$ , with as much DFSZ sensitivity achievable in 5 years of scan time, leading to the corner at  $\nu \approx 30 \text{ MHz}$  or  $m_a c^2 \approx 120 \text{ neV}$ .

An intriguing feature of the DMRadio- $m^3$  sensitivity is that the majority of the scan time is spent at lower masses above the DFSZ line. Above the  $120 \text{ neV}$  corner, the target  $g_{a\gamma\gamma}$  sensitivity increases  $\propto \nu$ , and the scan speed naively increases  $\propto \nu^3$  (see Eq. 6). The scan rate will be further enhanced because of the growth of  $\bar{\mathcal{G}}$ , due to the decreasing impact of thermal noise at higher frequencies – though this growth is slightly slower than  $\propto \nu_r$  (see Appendix A). This growth will be offset by a gradual decrease in  $Q$  and SQUID sensitivity at higher frequency.

#### V. CONCLUSION

The axion is one of the best theoretically motivated candidates to explain the DM abundance of the universe. At present, the parameter space of ADM models is relatively unexplored. Recent advances in superconducting quantum sensors, quantum acceleration protocols, and dilution refrigerator technology have made searching the full ADM parameter space more feasible than ever before. The region of ADM parameter space with  $m_a \lesssim 1 \mu\text{eV}$

is well motivated, and particularly attractive due to its connection with GUT models.

In this letter, we have presented the baseline design and sensitivity reach of the DMRadio- $m^3$  experiment, which uses a lumped element approach to search for QCD ADM over mass range  $20 \text{ neV} \lesssim m_a c^2 \lesssim 800 \text{ neV}$ . This design is capable of probing at or below the KSVZ sensitivity over the full range and DFSZ sensitivity above  $120 \text{ neV}$  with a 5 year scan time. This will make DMRadio- $m^3$  a key component in the next generation of experimental searches for ADM.

Future upgrades to DMRadio- $m^3$  could moderately extend the DFSZ sensitivity below the  $120 \text{ neV}$  corner through the use of backaction evading quantum sensors [68]. Future proposed experiments like DMRadio-GUT could probe DFSZ models to even lower masses through the use of beyond-SQL sensors and high-field, high-volume magnets [69].

#### ACKNOWLEDGMENTS

The authors acknowledge the support of from the NSF under awards 2110720 and 2014215. DMRadio- $m^3$  is supported by the DOE HEP Cosmic Frontier under FWP 100559. The study of resonator quality factor is supported under DOE HEP Detector R&D (award no. DE-SC0007968). DMRadio-50L is funded by the Gordon and Betty Moore Foundation. SLAC and UC Berkeley gratefully acknowledge support for this work from the Gordon and Betty Moore Foundation, grant number 7941. Additional support was provided by the Heising-Simons Foundation. S. Chaudhuri acknowledges support from the R.H. Dicke Postdoctoral Fellowship and Dave Wilkinson Fund at Princeton University. C. P. Salemi is supported in part by the National Science Foundation Graduate Research Fellowship under Grant No. 1122374. Y. Kahn is supported in part by DOE grant DE-SC0015655. B. R. Safdi was supported in part by the DOE Early Career Grant DESC0019225. P.W. Graham acknowledges support from the Simons Investigator Award no. 824870, DOE HEP QuantISED Award no. 100495, and the Gordon and Betty Moore Foundation Grant no. 7946. J. W. Foster was supported by a Pappalardo Fellowship.

#### Appendix A: Scan Rate Calculation

The general derivation of Eq. 6 and  $\bar{\mathcal{G}}$  can be found in [63]. Here we summarize the result for convenience.

In general, the voltage across an inductive pickup,  $L_{\text{PU}}$ , coupled to  $\mathbf{J}_{\text{eff}}$  will be proportional to the coupled energy  $U_{\text{DM}}$  [63]

$$|V_{pp}^2| = 4 \left( \frac{c^4}{\hbar^2} \right) m_a^2 L_{\text{PU}} U_{\text{DM}} \quad (\text{A1})$$

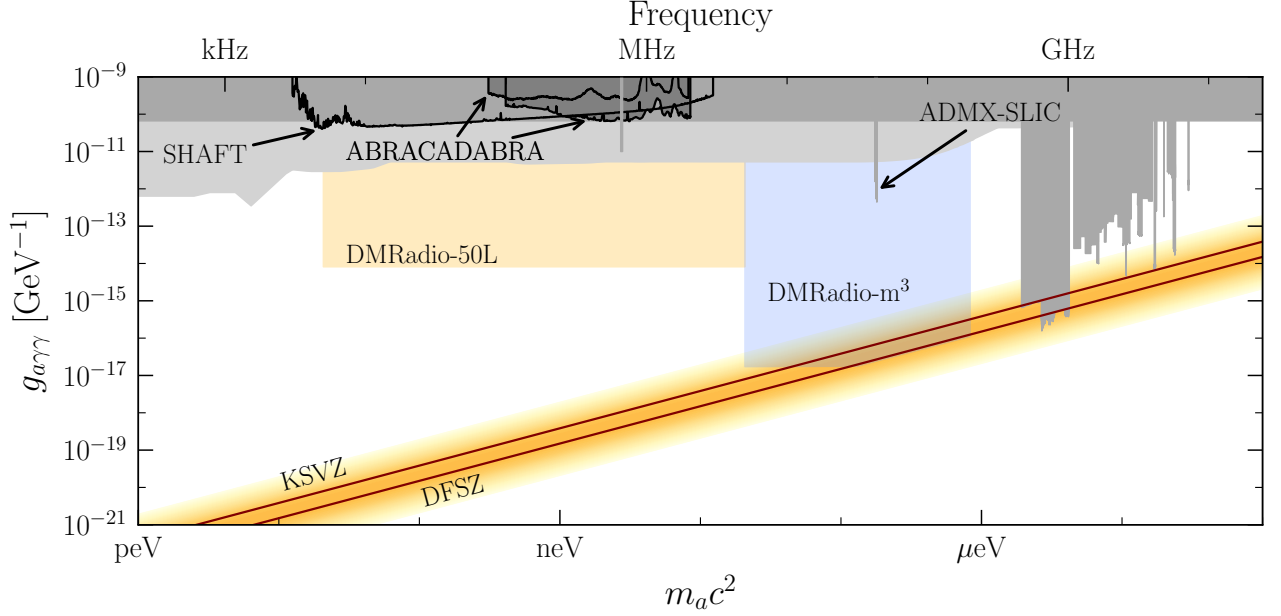


FIG. 3. Projected DMRadio- $m^3$  ADM search sensitivity with a 5 year scan, compared to projected sensitivity for DMRadio-50L, and existing bounds below  $1 \mu\text{eV}$  from ABRACADABRA-10 cm, SHAFT, ADMX-SLIC (narrow spike around  $200 \text{ neV}$ ), BASE (narrow spike around  $3 \text{ neV}$ ), and bounds from microwave cavity searches above  $1 \mu\text{eV}$ . DMRadio- $m^3$  targets at least KSVZ over the full search range, and DFSZ sensitivity above  $\approx 120 \text{ neV}$ . Plot generated using code modified from [67].

The coupled energy, defined as

$$U_{\text{DM}} = k^2 \frac{g_{a\gamma\gamma}^2 \rho_{\text{DM}}}{m_a^2} \frac{\hbar^3}{c \mu_0} \int_{V_{\text{PU}}} |\mathbf{B}(\mathbf{x})|^2 dV, \quad (\text{A2})$$

gives a measure of the amount of energy coupled from the axion field into the pickup. The dimensionless proportionality constant,  $k$ , is a geometric factor containing all the information about mutual coupling between the inductor and  $\mathbf{J}_{\text{eff}}$ . This constant generalizes the  $C_{nml}$  form factor in a cavity haloscope. Energy conservation dictates that  $k^2 \leq \frac{1}{2}$  [60]. However, it is also clear that the voltage driven across an inductive element should go to zero as the driving frequency goes to zero ( $m_a \rightarrow 0$ ), and that therefore  $k$  should have a dependence on  $m_a$ . Given this, it is convenient to define a new dimensionless constant,  $c_{\text{PU}}$ , that separates this mass dependence

$$k^2 = \left(\frac{c}{\hbar}\right)^2 m_a^2 V_{\text{PU}}^{2/3} \left( \frac{B_0^2 V_{\text{PU}}}{\int_{V_{\text{PU}}} |\mathbf{B}(\mathbf{x})|^2 dV} \right) c_{\text{PU}}^2 \quad (\text{A3})$$

and is both frequency and scale invariant. This constant can be calculated explicitly in the MQS limit, when the Compton wavelength is large compared to the size of the detector. In this limit, we can use the relationship  $V = \partial\Phi/\partial t$  and write  $\tilde{V}_{pp} = 2\pi\nu_a i\tilde{\Phi}_a$  in the frequency domain, where  $\Phi_a$  is the axion induced flux through the pickup. This flux can be extracted from the Biot-Savart law as

$$\Phi_a = g_{a\gamma\gamma} \sqrt{\hbar c} \sqrt{2\rho_{\text{DM}}} \cos\left(\frac{m_a c^2 t}{\hbar}\right) \times \int_A dA \int_{V_{\text{PU}}} dV' \hat{\mathbf{n}} \cdot \frac{\mathbf{B}_0(\mathbf{r}') \times (\mathbf{r} - \mathbf{r}')}{|\mathbf{r} - \mathbf{r}'|^3}. \quad (\text{A4})$$

where the integral  $dA$  is taken over the area of the pickup  $A$ , and the integral  $dV'$  is taken over the characteristic volume containing the pickup,  $V_{\text{PU}}$ . Combining Eqns. A1, A2, A3, and A4, we can write  $c_{\text{PU}}$  in the MQS limit as

$$c_{\text{PU}}^2 = \mu_0 \frac{\left| \int dA \int dV' \hat{\mathbf{n}} \cdot \frac{\mathbf{B}_0(\mathbf{r}') \times (\mathbf{r} - \mathbf{r}')}{|\mathbf{r} - \mathbf{r}'|^3} \right|^2}{2B_0^2 V_{\text{PU}}^{5/3} L_{\text{PU}}}. \quad (\text{A5})$$

The scale invariance can be seen explicitly by noting the scaling  $L_{\text{PU}} \propto V^{1/3}$  for a constant geometry. Typical values are  $c_{\text{PU}} \approx 0.1 - 0.2$ .

The resonant enhancement of the circuit comes directly from its impedance  $Z(\nu)$ . For a generic RLC circuit,  $Z(\nu) = R + i(2\pi\nu L + (2\pi\nu C)^{-1})$ , we can evaluate

$$\frac{1}{|Z(\nu)|^2} = \frac{Q^2}{4\pi^2 \nu_r^2 L^2 \left( 1 + Q^2 \frac{\nu_r^2}{\nu^2} \left( \frac{\nu^2}{\nu_r^2} - 1 \right)^2 \right)} \approx \frac{Q^2}{4\pi^2 \nu_r^2 L^2 (1 + 4Q^2 \Delta^2)} \quad (\text{A6})$$

where  $\nu_r = (2\pi\sqrt{LC})^{-1}$  and  $Q = \sqrt{L/CR^2}$ , and the approximation holds for  $\nu \approx \nu_r$ . We see the Lorentzian behavior of the resonator stems directly from the impedance of the readout circuit.

The noise power  $|\tilde{I}_N(\nu)|^2$  can be expressed in terms of a current noise power spectral density at the input coil of the readout SQUID,

$$S_{II}^{\text{tot}}(\nu) = \frac{|\tilde{I}_N(\nu)|^2}{\Delta\nu}. \quad (\text{A7})$$

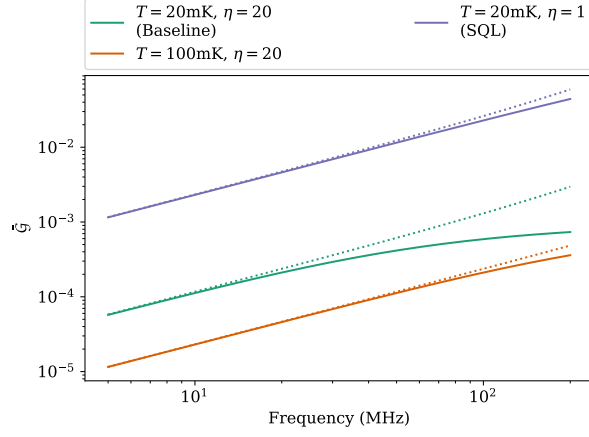


FIG. 4.  $\bar{G}(\nu, k_B T, \eta_A)$  as a function of frequency for several choices of physical temperature,  $T$ , and amplifier noise  $\eta_A$ . The solid lines show the full evaluation, while the dotted lines show the linear behavior, which holds for the region where  $k_B T / \hbar \nu \gg \frac{1}{2} \eta_A, 1$ .

This noise power can be decomposed into thermal, amplifier, and vacuum components

$$S_{II}^{\text{tot}}(\nu) = 8\pi\hbar\nu \left( n_T + \frac{1}{2} \right) \frac{\text{Re}[Z(\nu)]}{|Z(\nu)|^2} + S_{II}^{\text{Imp}} + \frac{S_{VV}^{\text{BA}}}{|Z(\nu)|^2} \quad (\text{A8})$$

Where the first term in the parenthesis corresponds to the number of thermal noise photons  $n_T(\nu, k_B T) = (\exp(2\pi\hbar\nu/k_B T) - 1)^{-1}$  at physical temperature  $T$ . DMRadio-m<sup>3</sup> targets a physical temperature of  $T = 20$  mK, corresponding to  $n_T \approx 90$  noise photons at 5 MHz and  $n_T \approx 2$  noise photons at 200 MHz. The  $\frac{1}{2}$  corresponds to the vacuum noise limit, intrinsic to any phase-insensitive measurement.  $S_{II}^{\text{Imp}}$  is the amplifier imprecision noise, expressed in terms of current noise at the amplifier input, and  $S_{VV}^{\text{BA}}$  is the amplifier backaction noise, expressed as a voltage source at the amplifier input and are both independent of frequency in this form. Equation A8 demonstrates the different spectral behavior of the various noise sources. The thermal, vacuum, and backaction noise are all shaped by the

resonator Lorentzian, while the imprecision noise has a spectrally flat distribution. In practice, a DC-SQUID will have an additional type of noise term,  $S_{IV}^{\text{corr}}$ , that defines correlations between the imprecision and backaction noise [70, 71]. These correlations complicate the optimization and are included in our sensitivity calculation, but do not qualitatively change the approach and so are omitted here for simplicity.

The amplifier noise parameter,  $\eta_A$  can be written in terms of these noise powers as

$$\eta_A = \frac{\sqrt{S_{II}^{\text{Imp}} S_{VV}^{\text{BA}}}}{2\pi\hbar\nu}. \quad (\text{A9})$$

At the SQL,  $\eta_A = 1$ . For DMRadio-m<sup>3</sup>, the amplifier noise target is  $\eta_A = 20$ , including the correlated noise that we have omitted here. This corresponds to  $n_A = \eta_A/2 = 10$  added noise photons.

The amplifier noise parameter  $\eta_A$  depends on the amplifier imprecision and backaction noise as well as  $\kappa$  coupling in Fig. 2, which regulates the tradeoff between the two. In particular,  $S_{II}^{\text{Imp}} \propto \eta_A/\kappa^2$ , while  $S_{VV}^{\text{BA}} \propto \eta_A \kappa^2$ . A stronger coupling increases the backaction noise and decreases the input referred imprecision noise. Because of the different spectral responses of these two noise terms, the coupling  $\kappa$  can be optimized to give the fastest possible scan rate. For a careful and extensive analysis of this optimization, including noise correlations, see [63]. But the resulting effect on the scan rate can be written in terms of a single parameter

$$\bar{G}(\nu_r, \bar{\alpha}, k_B T, \eta_A) = \frac{\bar{\alpha}}{[\bar{\alpha}^2 + 2(2n_T + 1)\bar{\alpha} + \eta_A^2]^{3/2}} \quad (\text{A10})$$

where

$$\bar{\alpha} = \frac{2\eta_A^2}{2n_T + 1 + \sqrt{(2n_T + 1)^2 + 8\eta_A^2}}. \quad (\text{A11})$$

In the Raleigh-Jeans limit, where  $n_T \gg \frac{1}{2}\eta_A, 1$  or equivalently  $k_B T / \hbar \nu \gg \frac{1}{2}\eta_A, 1$ ,  $\bar{G}$  has an approximately linear dependence on  $\nu$ :

$$\bar{G} \approx \frac{2\pi\hbar\nu}{6\sqrt{3}k_B T \eta_A}, \quad \frac{k_B T}{\hbar\nu} \gg \frac{1}{2}\eta_A, 1. \quad (\text{A12})$$

[1] R. D. Peccei and H. R. Quinn, *Phys. Rev.* **D16**, 1791 (1977).  
[2] R. D. Peccei and H. R. Quinn, *Phys. Rev. Lett.* **38**, 1440 (1977).  
[3] S. Weinberg, *Phys. Rev. Lett.* **40**, 223 (1978).  
[4] F. Wilczek, *Phys. Rev. Lett.* **40**, 279 (1978).  
[5] S. Borsanyi *et al.*, *Nature* **539**, 69 (2016), [arXiv:1606.07494 \[hep-lat\]](#).  
[6] L. F. Abbott and P. Sikivie, *Phys. Lett. B* **120**, 133 (1983).

[7] J. Preskill, M. B. Wise, and F. Wilczek, *Phys. Lett. B* **120**, 127 (1983).  
[8] M. Dine and W. Fischler, *Phys. Lett. B* **120**, 137 (1983).  
[9] M. Tegmark, A. Aguirre, M. Rees, and F. Wilczek, *Phys. Rev. D* **73**, 023505 (2006), [arXiv:astro-ph/0511774](#).  
[10] M. P. Hertzberg, M. Tegmark, and F. Wilczek, *Phys. Rev. D* **78**, 083507 (2008), [arXiv:0807.1726 \[astro-ph\]](#).  
[11] R. T. Co, F. D’Eramo, and L. J. Hall, *Phys. Rev. D* **94**, 075001 (2016), [arXiv:1603.04439 \[hep-ph\]](#).  
[12] P. W. Graham and A. Scherlis, *Phys. Rev. D* **98**, 035017

- (2018), [arXiv:1805.07362 \[hep-ph\]](#).
- [13] F. Takahashi, W. Yin, and A. H. Guth, *Phys. Rev. D* **98**, 015042 (2018).
  - [14] L. Di Luzio, M. Giannotti, E. Nardi, and L. Visinelli, *Phys. Rept.* **870**, 1 (2020), [arXiv:2003.01100 \[hep-ph\]](#).
  - [15] R. T. Co, F. D'Eramo, and L. J. Hall, *Phys. Rev. D* **94**, 075001 (2016).
  - [16] M. B. Wise, H. Georgi, and S. L. Glashow, *Phys. Rev. Lett.* **47**, 402 (1981).
  - [17] G. Ballesteros, J. Redondo, A. Ringwald, and C. Tamarit, *JCAP* **08**, 001, [arXiv:1610.01639 \[hep-ph\]](#).
  - [18] A. Ernst, A. Ringwald, and C. Tamarit, *JHEP* **02**, 103, [arXiv:1801.04906 \[hep-ph\]](#).
  - [19] L. Di Luzio, A. Ringwald, and C. Tamarit, *Phys. Rev. D* **98**, 095011 (2018), [arXiv:1807.09769 \[hep-ph\]](#).
  - [20] A. Ernst, L. Di Luzio, A. Ringwald, and C. Tamarit, *PoS CORFU2018*, 054 (2019), [arXiv:1811.11860 \[hep-ph\]](#).
  - [21] P. Fileviez Pérez, C. Murgui, and A. D. Plascencia, *JHEP* **11**, 093, [arXiv:1908.01772 \[hep-ph\]](#).
  - [22] P. Fileviez Pérez, C. Murgui, and A. D. Plascencia, *JHEP* **01**, 091, [arXiv:1911.05738 \[hep-ph\]](#).
  - [23] P. Svrcek and E. Witten, *JHEP* **06**, 051, [arXiv:hep-th/0605206](#).
  - [24] M. B. Green and J. H. Schwarz, *Phys. Lett. B* **149**, 117 (1984).
  - [25] J. P. Conlon, *JHEP* **05**, 078, [arXiv:hep-th/0602233](#).
  - [26] B. S. Acharya, K. Bobkov, and P. Kumar, *JHEP* **11**, 105, [arXiv:1004.5138 \[hep-th\]](#).
  - [27] A. Ringwald, *J. Phys. Conf. Ser.* **485**, 012013 (2014), [arXiv:1209.2299 \[hep-ph\]](#).
  - [28] M. Cicoli, M. Goodsell, and A. Ringwald, *JHEP* **10**, 146, [arXiv:1206.0819 \[hep-th\]](#).
  - [29] J. Halverson, C. Long, B. Nelson, and G. Salinas, *Phys. Rev. D* **100**, 106010 (2019), [arXiv:1909.05257 \[hep-th\]](#).
  - [30] E. Witten, *Phys. Lett. B* **149**, 351 (1984).
  - [31] M. Tegmark, A. Aguirre, M. J. Rees, and F. Wilczek, *Phys. Rev. D* **73**, 023505 (2006).
  - [32] R. T. Co, L. J. Hall, and K. Harigaya, *Journal of High Energy Physics* **2021**, 172 (2021).
  - [33] J. E. Kim, *Phys. Rev. Lett.* **43**, 103 (1979).
  - [34] M. Shifman, A. Vainshtein, and V. Zakharov, *Nucl. Phys. B* **166**, 493 (1980).
  - [35] M. Dine, W. Fischler, and M. Srednicki, *Phys. Lett. B* **104**, 199 (1981).
  - [36] A. Zhitnitsky, *Sov. J. Nucl. Phys.* **31**, 260 (1980).
  - [37] P. Sikivie, *Phys. Rev. Lett.* **51**, 1415 (1983), [Erratum: *Phys. Rev. Lett.* **52**, 695 (1984)].
  - [38] J. Herzog-Arbeitman, M. Lisanti, P. Madau, and L. Necib, *Phys. Rev. Lett.* **120**, 041102 (2018), [arXiv:1704.04499 \[astro-ph.GA\]](#).
  - [39] P. F. de Salas and A. Widmark, *Reports on Progress in Physics* **84**, 104901 (2021).
  - [40] C. Hagmann, P. Sikivie, N. S. Sullivan, and D. B. Tanner, *Physical Review D* **42**, 1297(r) (1990).
  - [41] S. J. Asztalos *et al.* (ADMX), *Phys. Rev. D* **64**, 092003 (2001).
  - [42] T. Braine *et al.* (ADMX Collaboration), *Phys. Rev. Lett.* **124**, 101303 (2020).
  - [43] C. Bartram *et al.* (ADMX Collaboration), *Phys. Rev. Lett.* **127**, 261803 (2021).
  - [44] B. M. Brubaker *et al.*, *Phys. Rev. Lett.* **118**, 061302 (2017).
  - [45] K. M. Backes *et al.*, *Nature* **590**, 238 (2021).
  - [46] D. Alesini *et al.*, *Phys. Rev. D* **103**, 102004 (2021).
  - [47] S. Lee, S. Ahn, J. Choi, B. R. Ko, and Y. K. Semertzidis, *Phys. Rev. Lett.* **124**, 101802 (2020).
  - [48] B. Cabrera and S. Thomas, *Workshop Axions 2010*, U. Florida (2008).
  - [49] P. Sikivie, N. Sullivan, and D. B. Tanner, *Phys. Rev. Lett.* **112**, 131301 (2014).
  - [50] Y. Kahn, B. R. Safdi, and J. Thaler, *Phys. Rev. Lett.* **117**, 141801 (2016).
  - [51] S. Chaudhuri *et al.*, *Phys. Rev. D* **92**, 075012 (2015).
  - [52] M. Silva-Feaver, S. Chaudhuri, H. Cho, C. Dawson, P. Graham, K. Irwin, S. Kuenstner, D. Li, J. Mardon, H. Moseley, R. Mule, A. Phipps, S. Rajendran, Z. Stefan, and B. Young, *IEEE Transactions on Applied Superconductivity* **27**, 1 (2017).
  - [53] J. L. Ouellet *et al.*, *Phys. Rev. Lett.* **122**, 121802 (2019).
  - [54] J. L. Ouellet *et al.*, *Phys. Rev. D* **99**, 052012 (2019).
  - [55] C. P. Salemi, J. W. Foster, J. L. Ouellet, *et al.*, *Phys. Rev. Lett.* **127**, 081801 (2021).
  - [56] A. V. Gramolin *et al.*, *Nature Physics* **10.1038/s41567-020-1006-6** (2020).
  - [57] N. Crisosto, P. Sikivie, N. S. Sullivan, D. B. Tanner, J. Yang, and G. Rybka, *Phys. Rev. Lett.* **124**, 241101 (2020).
  - [58] J. A. Devlin *et al.*, *Phys. Rev. Lett.* **126**, 041301 (2021).
  - [59] A. Phipps *et al.*, in *Microwave Cavities and Detectors for Axion Research*, edited by G. Carosi and G. Rybka (Springer International Publishing, Cham, 2020) pp. 139–145.
  - [60] S. Chaudhuri, *J. Cosmol. Astropart. Phys.* **2021**, 033 (2021).
  - [61] L. Brouwer *et al.* (DMRadio Collaboration), Search for Axion Dark Matter Below  $1\mu\text{eV}$  with DMRadio-50L (2022), (Paper in preparation).
  - [62] L. Brouwer *et al.* (DMRadio Collaboration), Lumped Element Search for Dark Matter Detectors: Toroidal vs Solenoidal Configuration (2022), (Paper in preparation).
  - [63] S. Chaudhuri, K. Irwin, P. W. Graham, and J. Mardon, (2018), [arXiv:1803.01627 \[hep-ph\]](#).
  - [64] P. Falferi *et al.*, *Appl. Phys. Lett.* **93**, 172506 (2008), <https://doi.org/10.1063/1.3002321>.
  - [65] C. Alduino *et al.*, *Cryogenics* **102**, 9 (2019).
  - [66] D. Q. Adams *et al.* (CUORE), *Nature* **604**, 53 (2022).
  - [67] C. O'Hare, *cajohare/axionlimits: Axionlimits*, <https://cajohare.github.io/AxionLimits/> (2020).
  - [68] A. A. Clerk, F. Marquardt, and K. Jacobs, *New Journal of Physics* **10**, 095010 (2008).
  - [69] L. Brouwer *et al.* (DMRadio Collaboration), (2022), [arXiv:2203.11246 \[hep-ex\]](#).
  - [70] W. Myers *et al.*, *Journal of Magnetic Resonance* **186**, 182 (2007).
  - [71] A. A. Clerk, M. H. Devoret, S. M. Girvin, F. Marquardt, and R. J. Schoelkopf, *Rev. Mod. Phys.* **82**, 1155 (2010).